Available online at www.sciencedirect.com
ScienceDirect
Cement and Concrete Research 36 (2006) 1523–1532
Cement and Concrete Research

Crystallized alkali-silica gel in concrete from the late 1890s

Karl Peterson [a,*], David Gress [b], Tom Van Dam [a], Lawrence Sutter [a]

[a] Department of Civil and Environmental Engineering, Michigan Technological University, Houghton, Michigan, USA
[b] Civil Engineering Department, University of New Hampshire, Durham, New Hampshire, USA

Received 1 September 2005; accepted 22 May 2006

Abstract

The Elon Farnsworth Battery, a concrete structure completed in 1898, is in an advanced state of disrepair. To investigate the potential for rehabilitation, cores were extracted from the battery. Petrographic examination revealed abundant deposits of alkali silica reaction products in cracks associated with the quartz rich metasedimentary coarse aggregate. The products of the alkali silica reaction are variable in composition and morphology, including both amorphous and crystalline phases. The crystalline alkali silica reaction products are characterized by quantitative X-ray energy dispersive spectrometry (EDX) and X-ray diffraction (XRD). The broad extent of the reactivity is likely due to elevated alkali levels in the cements used.

Keywords: Alkali-aggregate reaction; Petrography; SEM; EDX; X-ray diffraction

1. Introduction

The Elon Farnsworth Battery has overlooked the entrance to Portsmouth Harbor for over 100 years. Artillery has been part of the landscape since 1631, when the first guns were installed in an earthen redoubt [1,2]. Placement of the concrete for Farnsworth Battery began in 1897, at a time when the use of Portland cement was gaining in popularity over the more commonly used natural cements [natural cement, or "rock cement" was typically produced from a single source of limestone that contained enough impurities to create a product similar to modern Portland cement] [7]. The history of the construction of the battery was preserved in the lettercopy book of Inspector J.W. Walker. Excerpts from his notes, compiled by Perrault and Ofenstein in a historical report on the battery, reveal that two natural cements from the New York Rosendale District were used during construction, Hoffman Cement and Beach's Cement, as well as one Portland cement from the Pennsylvania Lehigh Valley, Atlas Cement [3]. The natural cements were primarily used in the bulk concrete of the parapet. The Portland cement was reserved for the remaining concrete construction [3]. Table 1 lists chemical compositions for the three cements, as reported in literature from the period [4,5]. The most striking compositional difference between the cements is the high MgO content of the natural cements versus the Portland cement, (Table 1). Also of interest in Table 1 is the high level of alkalies reported for the Hoffman Cement. Natural cement from the Rosendale District was widely used in the 1800s and early 1900s. By the 1920s, Portland cement dominated cement production, and the use of natural cement declined [6]. In the late 1890s, there were at least fifteen different

Table 1
Chemical compositions of cement as reported in literature

Oxide wt.%	Hoffman cement, Cummings (1898)	Beach's cement, Eckel (1905)	Atlas cement, Eckel (1905)
SiO_2	27.3	27.75	21.3
Al_2O_3	7.14	5.5	7.65
Fe_2O_3	1.8	4.28	2.85
MgO	18	21.18	2.95
CaO	35.98	35.61	60.95
K_2O, Na_2O	6.8	trace	1.15
SO_3	*	0.5	1.81
CO_2	*	4.05	*
H_2O	*	*	*
LOI	2.98	*	*
Sum	100	98.87	98.66

*Not determined.

* Corresponding author.
E-mail addresses: cee@mtu.edu (K. Peterson), dlgress@unh.edu (D. Gress), cee@mtu.edu (T. Van Dam), cee@mtu.edu (L. Sutter).

0008-8846/$ - see front matter © 2006 Elsevier Ltd. All rights reserved.
doi:10.1016/j.cemconres.2006.05.017

Fig. 1. Gun position number 1 of the Farnsworth Battery, soon after construction in 1898, photo from personal collection of Bolling Smith.

companies producing natural cement in the Rosendale District, but the practices of the Lawrence Cement Company, producer of the Hoffman brand, are well documented and briefly described here [4,8]. The rock used in Hoffman cement was quarried from a blend of an upper, light colored limestone, and a lower, dark colored limestone, both separated by a layer of sandstone. In the morning, alternating layers of crushed rock and anthracite pea coal were fed into the top of a 3 m dia. by 8.5 m high kiln, and burnt overnight. The following morning, the burnt product was discharged from the base of the kiln and sorted. Over-burnt rock was discarded, and under-burnt rock was returned to the top of the kiln. Properly calcined rock was crushed, ground, and packaged in barrels. The practices of cement production in the Rosendale District remained relatively unchanged since its inception in the 1830s. Atlas Cement of the 1890s, on the other hand, represented the latest in cement technology, and was the first successful Portland cement produced in the United States by rotary kiln [9,10]. The coarse aggregate used in the battery, a quartz rich metasedimentary rock, originated from crushed material excavated from the site. The fine aggregate, according to the inspector's notes, was shipped from Plum Island, Massachusetts, a source 30 km to the south [3]. Also according to the inspector's notes, water for the concrete mix, as well as for moist curing, was taken directly from the harbor [3]. After completion of the battery, it was noticed that the guns in their retracted position protruded as much as 20 cm above the parapet, so, in 1903, an additional 23 cm of concrete was added to the parapet apron [3]. Fig. 1 shows the battery as armed in 1898. The battery experienced structural and moisture problems soon after construction, and the guns were removed during World War I. In 1948, the fort was deactivated

Fig. 2. Current condition of gun position number 2 of the Farnsworth Battery, (gun removed) photo from Pete Payette, American Forts Network.

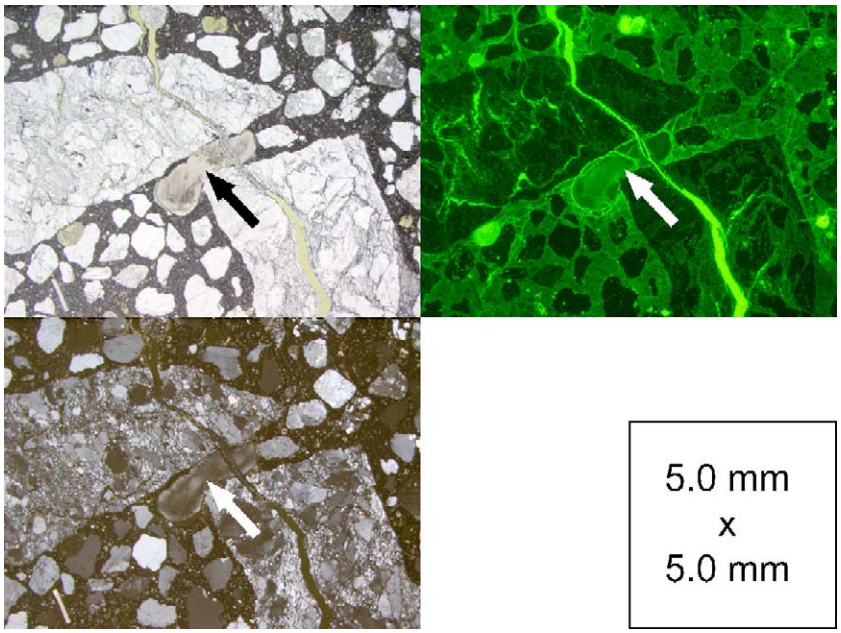

Fig. 3. Crystallized gel deposit (arrow) between two coarse aggregate particles, clockwise from upper left: plane polarized, epifluorescent mode, and crossed polars.

[11]. In 2001, a 2 ha parcel of land, including the battery, was transferred to the University of New Hampshire (UNH). To assess the condition of the battery, cores were collected from the concrete in 2003. Fig. 2 shows the current condition of the battery.

It is widely accepted that the production of alkali silica gel plays the primary role in the deleterious nature of the alkali silica reaction. Alkali silica gels may crystallize over time, and observations of crystalline alkali silica reaction products have been reported throughout the literature [12–23]. Most researchers attribute the presence of crystalline alkali silica reaction products to the crystallization of alkali silica gel. A variety of mechanisms have been reported to explain the crystallization. Some researchers have found that crystallization requires the drying of the gel. Cole and Lancucki reported the crystallization of gel after heating to 110 °C, followed by a period of 12 days at ambient room conditions [13]. Fernandes et al. describe a gel that crystallizes over time when kept in a desiccation chamber [22]. Some researchers have reported compositional differences between gels and crystallized gels [15–22]. Thordal Anderson and Thaulow, and Thaulow et al. noted that crystallized gels are often observed in cracks within the aggregate, and less often observed in cracks within the cement paste [17,18]. They suggest that compositional differences between the crystallized gel and the amorphous gel may be due to local differences in the pore

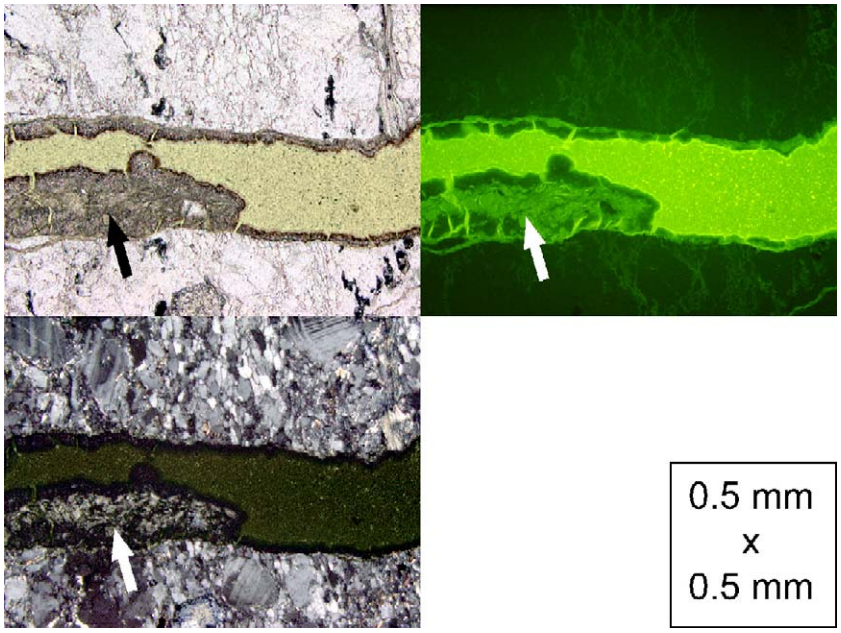

Fig. 4. Crystallized gel (arrow) in crack in coarse aggregate particle, clockwise from upper left: plane polarized, epifluorescent mode and crossed polars.

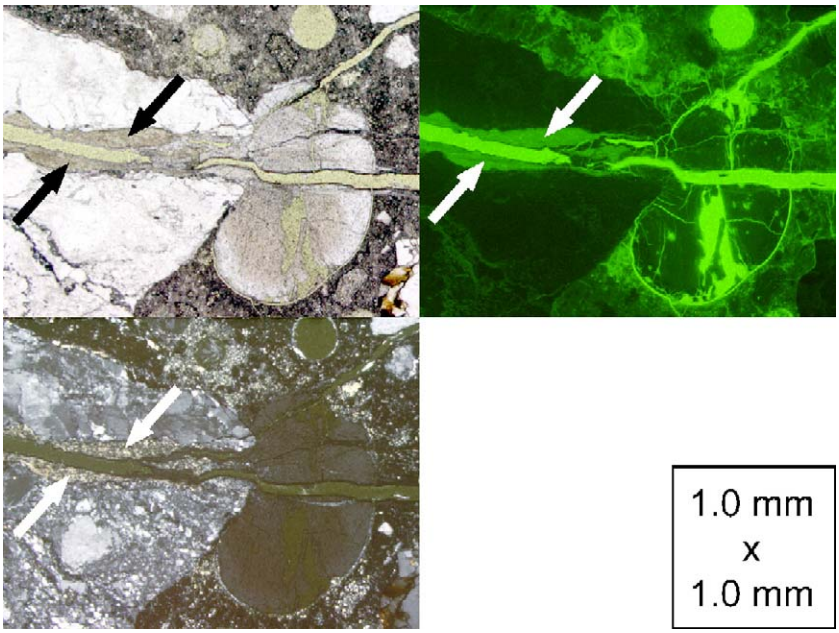

Fig. 5. Crystallized gel lined crack, (arrows) in coarse aggregate particle, and amorphous gel deposit within cement paste, clockwise from upper left: plane polarized, epifluorescent mode, and crossed polars.

water chemistry within the aggregate versus the pore water chemistry within the cement paste. Kurtis et al. describe an experiment where the crystallization of alkali silica gel is observed in situ via soft X-ray transmission microscopy when immersed in solutions of calcium and sodium hydroxide [19,20]. It is the experience of the authors that the quantities of crystallized gel observed in concrete are generally limited as compared to normal, or amorphous alkali silica gel. However, crystallized gel is abundant in the concrete of Farnsworth Battery, and is present in quantities suitable for collection and study. The characterization of the crystallized gel is the primary focus of this paper.

2. Experimental

Four cores were received in an air dry state: two from the shell room beneath gun position number 1, one from the parapet apron in front of gun position number 1, and one from the floor adjacent to gun position number 1. An additional half core, split during unconfined compressive strength testing by UNH, from the parapet wall adjacent to gun position number 1 was also received. Macro examination of the cores showed abundant cracks and voids filled with white alkali silica reaction product. The core from the floor adjacent to the gun position was stabilized by vacuum impregnation with fluorescent dyed epoxy. After impregnation, the excess epoxy was used to stabilize the core from the apron by pouring into visible cracks. Both cores were cut into slabs with a kerosene cooled diamond saw. One of the slabs cut from the parapet apron core was used to collect scrapings of alkali silica reaction product for XRD. Prisms were cut from the slabs from the gun placement floor, and prepared in thin section using water free preparation methods. The final thickness of the thin sections was 30 μm, and the final polish was completed with 0.25 μm diamond grit.

To examine fresh fracture faces, a hammer was used to shatter the split core from the parapet wall. A chip of concrete with a deposit of alkali silica reaction product was collected and examined in water vapor mode with a Philips XL40 environmental scanning electron microscope (ESEM) equipped with an EDAX EDS detector at a pressure of 1 Torr, an accelerating voltage of 20 kV, and a beam current of 1 nA.

The thin sections were cleaned with 200 proof ethanol, carbon coated, and examined in high vacuum mode with the Philips XL40 ESEM. EDX measurements were made at an accelerating voltage of 15 kV, and a beam current of 0.6 nA, using EDAX Phoenix SEM QUANT ZAF software and mineral standards. As a first approximation, 0.2 wt.% oxide is assumed as the detection limit for all oxide phases analyzed.

The scrapings of alkali silica reaction product from the parapet apron core were fixed to a nylon fiber with clear fingernail polish. The specimen was mounted in a Philips Electron Instruments, Inc. 28.65 mm radius Debye–Scherrer powder diffraction camera equipped with a mechanism for rotation of the specimen during

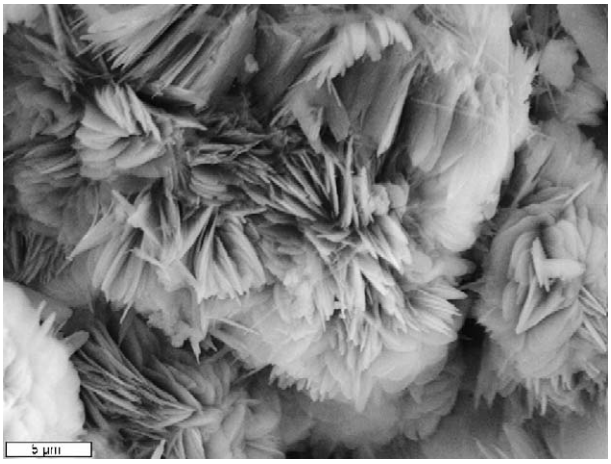

Fig. 6. Crystallized gel from fresh fracture surface, GSE image.

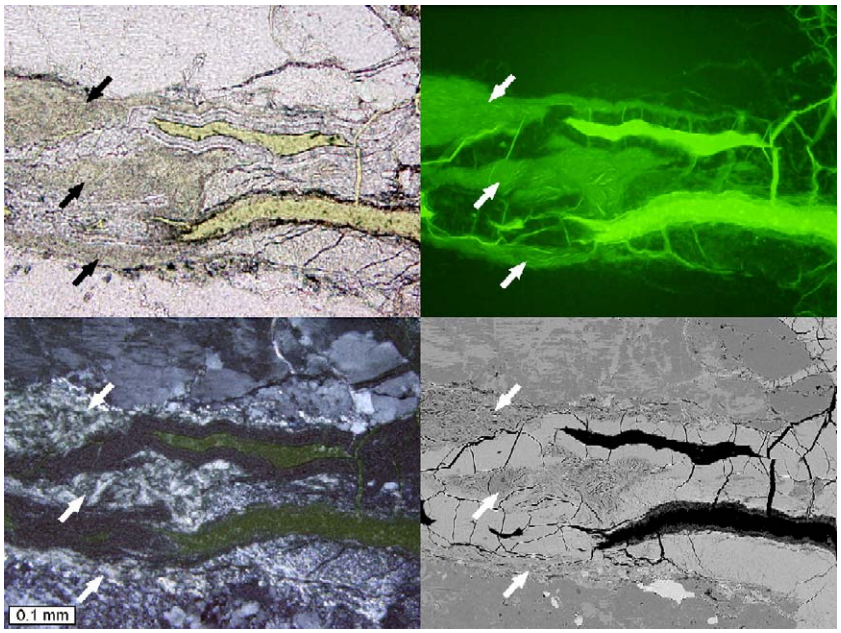

Fig. 7. Crystallized gel, (arrows) and amorphous gel in a crack, clockwise from upper left: plane polarized, epifluorescent mode, crossed polars, and BSE image.

pattern collection. The film was mounted via the Straumanis method, and the exposure time was 4 h. Cu Ka radiation was produced with a Philips Electron Instruments, Inc. generator at an accelerating voltage of 40 kV, a current of 20 mA, and a Ni filter. The resolution of the recorded pattern, that is, the shortest discernable distance between neighboring diffraction lines on the film, is estimated to be on the order of 0.2 mm, which translates into a 2 theta angle of 0.1°.

3. Results

3.1. Petrographic microscope observations

Figs. 3–5 show deposits of alkali silica reaction products as observed in thin section. In Fig. 3, a large deposit of crystallized gel is situated between two coarse aggregate particles. In Fig. 4, a crystallized gel deposit sits in a crack within a coarse aggregate particle. Fig. 5 shows a large crack through a coarse aggregate particle. The crack exits the aggregate, and extends into a large gel deposit within a void in the cement paste. In Fig. 5, crystallized gel lines the sides of the crack within the coarse aggregate, whereas the large deposit within the cement paste contains primarily amorphous gel.

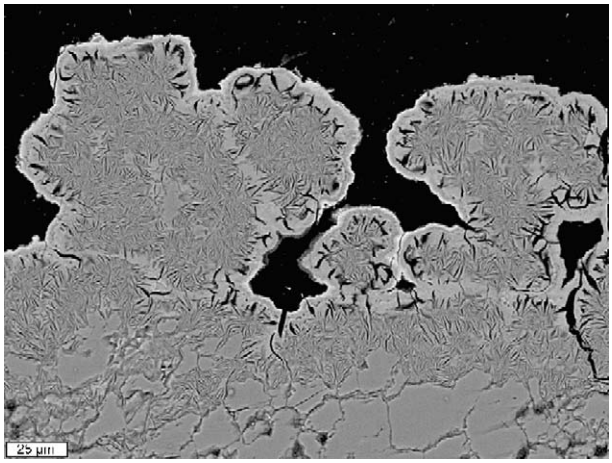

Fig. 8. Crystallized gel deposit, BSE image.

3.2. Environmental SEM observations

Fig. 6 shows the bladed structure of the crystallized gel in gaseous secondary electron (GSE) image mode. The blades are on the order of 1 µm in thickness, 5 to 10 µm in width and breadth, and protrude at a variety of orientations.

Table 2
Summary of EDX measurements from 10 measurements of crystallized gel, 10 measurements of amorphous gel adjacent to crystallized gel, and 10 measurements of amorphous gel away from the crystallized gel

Oxide wt.%	Xtal gel avg	Xtal gel S.D.	Gel adj to xtal avg	Gel adj to xtal S.D.	Gel avg	Gel S.D.	Okenite	Nekoite	Cole and Lanc. (1983)
SiO_2	54.1	2.0	54.7	3.6	49.6	4.6	55.0	55.1	59.9
TiO_2	0.0	0.0	0.0	0.0	0.0	0.0	0.0	0.0	–
Al_2O_3	0.2	0.1	0.1	0.0	0.3	0.2	0.0	0.0	3.8
Fe_2O_3	0.1	0.1	0.1	0.1	0.1	0.1	0.0	0.0	–
MnO	0.1	0.0	0.1	0.1	0.1	0.1	0.0	0.0	–
MgO	0.0	0.0	0.0	0.0	0.0	0.0	0.0	0.0	–
CaO	18.0	2.0	28.4	3.6	33.4	4.3	28.5	25.7	18.5
Na_2O	2.1	0.8	1.2	0.3	0.5	0.3	0.0	0.0	3.1
K_2O	7.2	0.7	3.3	0.8	1.2	0.7	0.0	0.0	4.7
P_2O_5	0.1	0.1	0.1	0.0	0.2	0.1	0.0	0.0	–
SO_3	0.1	0.1	0.1	0.1	0.1	0.1	0.0	0.0	–
Cl	0.1	0.1	0.0	0.0	0.0	0.0	0.0	0.0	–
Sum	82.1	3.5	88.1	4.9	85.5	3.6	100.0	100.0	103.5
H_2O*	17.9	3.5	11.9	4.9	14.5	3.6	16.5	19.3	13.6

*Not included in quantitative EDX measurements, computed as difference from 100 wt.%.

Table 3
Summary of EDX measurements from the crystallized gel recast as mineral formula based on 32 anions, (as per okenite) and recast as mineral formula based on 22 anions, (as per nekoite)

	32 anion basis				22 anion basis			
Ion	Xtal gel avg	Xtal gel S.D.	Okenite	Cole and Lanc. (1983)	Xtal gel avg	Xtal gel S.D.	Nekoite	Cole and Lanc. (1983)
Si^{+4}	8.90	0.57	9	9.70	6.12	0.39	6	6.67
Ti^{+4}	0.00	0.00		–	0.00	0.00		–
Al^{+3}	0.05	0.02		0.72	0.03	0.01		0.50
Fe^{+2}	0.01	0.01		–	0.00	0.01		–
Mn^{+2}	0.01	0.01		–	0.01	0.00		–
Mg^{+2}	0.00	0.01		–	0.00	0.00		–
Ca^{+2}	3.18	0.44	5	3.21	2.18	0.30	3	2.21
Na^{+1}	0.67	0.26		0.97	0.46	0.18		0.67
K^{+1}	1.52	0.17		0.97	1.04	0.12		0.67
PO_4^{-3}	0.02	0.01		–	0.01	0.01		–
SO_4^{-2}	0.01	0.01		–	0.01	0.00		–
Cl^{-1}	0.03	0.01		–	0.02	0.01		–
O^{-2}	31.89	0.04	32	32.00	21.92	0.03	22	22.00
H^{+1}	19.54	3.13	18	14.68	13.44	2.15	14	10.09
H_2O	9.77	1.56	9	7.34	6.72	1.08	7	5.05

3.3. High vacuum SEM observations

The region shown in Fig. 5 was chosen for further study because both crystallized and amorphous gel were present in large quantities. Fig. 7 shows a close up of the area in Fig. 5, just where the large crack exits the aggregate and reaches the cement paste. In the plane polarized image of Fig. 7, the laminar morphology of the amorphous is apparent. The bladed appearance of the crystallized gel, as demonstrated in Fig. 6, is represented in cross section in the back scattered electron (BSE) image of Fig. 8. The gaps between the crystals are due to the bladed morphology of the crystallized gel, but may also be partially accounted for by desiccation. The crystallized gel shown in Fig. 8 lines a crack within a coarse aggregate, in a region similar to that shown in Fig. 4. EDX measurements were made on the crystallized gel and the amorphous gel shown in Figs. 5 and 7. The measurements were made in three groups: crystallized gel, amorphous gel adjacent to crystallized gel, and amorphous gel away from crystallized gel. Table 2 summarizes the measurements from the three groups. In Table 2, the measurements are compared to computed compositions for pure okenite, ($Ca_5Si_9O_{23}\cdot 9H_2O$) and nekoite, ($Ca_3Si_6O_{15}\cdot 7H_2O$) a closely related mineral [24]. In Table 2, the measurements are also compared to values for a crystallized gel reported by Cole and Lancucki [13]. Table 3 shows a summary of the measurements from the crystallized gel recast as mineral formulas based on 32 and 22 anions and compared to the formulas for okenite and nekoite respectively. Mineral formula calculations were performed according to procedures described by Deer et al. [25]. Water was not included in the quantitative analysis, but is computed in Table 2 as the difference between the sum of the oxide wt.% values and 100. Carbonate was not included in the analysis due to the difficulty of carbon determination on a carbon

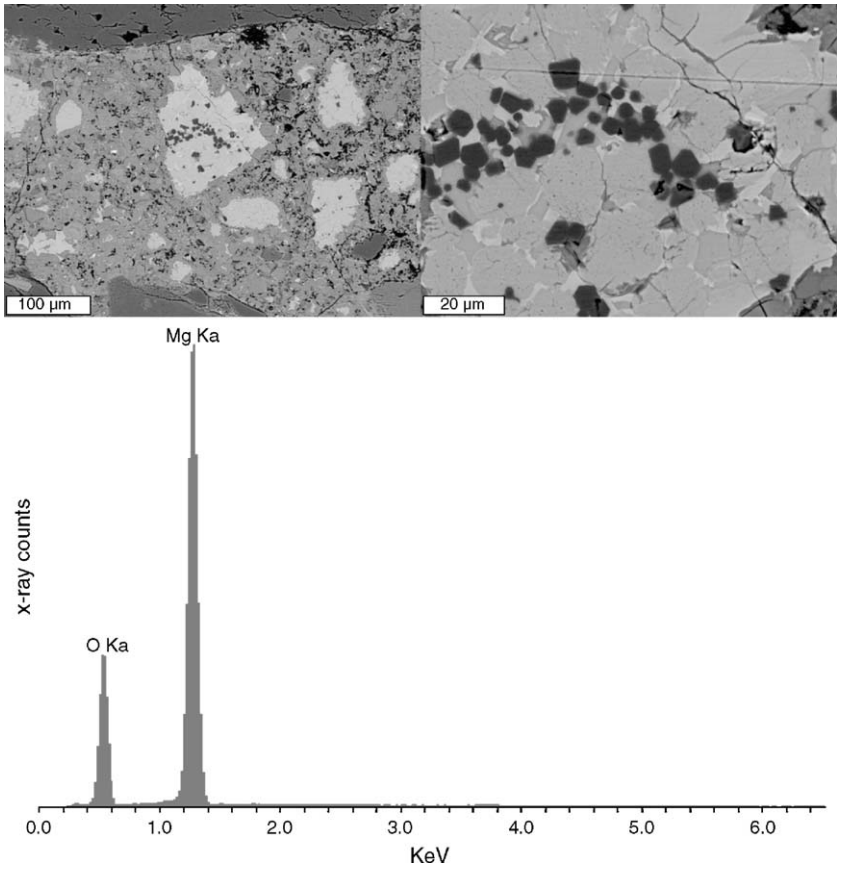

Fig. 9. BSE images of cement grain with dark periclase crystals, and EDS collected from periclase crystal, *y*-axis is in arbitrary units of X-ray counts.

coated sample. Although carbonate may be present in the crystallized gel, it is neglected here. The mineral formula values for H_2O listed in Table 3 were determined using the computed H_2O wt.% values from Table 2.

Fig. 9 shows BSE images of a large cement grain with an unhydrated interior. In the cement grain, there are a large number of angular dark crystals, likely periclase. The lower portion of Fig. 9 includes an X-ray energy dispersive spectra, (EDS) collected from one of the dark crystals, and shows large peaks for Mg Ka and O Ka radiation. No point counting, or quantitative work was done to determine MgO content of the cement.

3.4. X-ray diffraction

Fig. 10 shows the XRD pattern collected from the deposit of alkali silica reaction product. The pattern shows maximum intensity peaks at 8.4 and 3.6 Å, and major peaks at 10.6, 6.4, 4.3, 3.6, and 2.9 Å. The pattern is similar to patterns collected by Cole and Lancucki from crystallized gel [13]. Tables 4a and 4b compare the spacings and intensities reported by Cole and Lancucki for their crystallized gel, the crystallized gel from the battery, for okenite, (ICCD PDF 33–305) and for nekoite, (ICCD PDF 31–303).

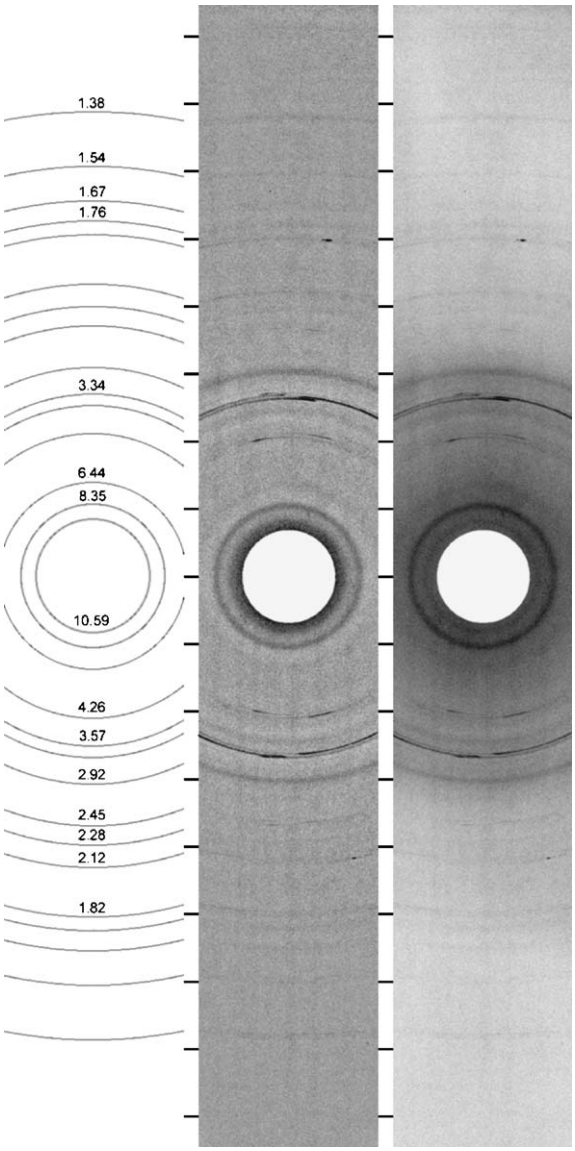

Fig. 10. From top right to bottom left: XRD pattern collected from crystallized gel, same pattern after high-pass filter, and a *d*-spacing labeled pattern, (in angstroms) where each label refers to the line positioned to the immediate right immediately below, scale bar tic marks every 1 cm.

4. Discussion and conclusions

The chemical composition of the crystallized alkali silica gel from Battery Farnsworth is similar to the chemical composition of crystallized gel reported by Cole and Lancucki, which they identified as okenite, with K and Na substitutions [13]. However, there are some questions whether the okenite structure could accommodate such extensive substitution of monovalent K^{+1} and Na^{+1} for divalent Ca^{+2}. The mineral formula of the crystallized gel from the battery, based on 32 anions, was computed to be $(Ca, Na, K)_{5.4}(Si, Al)_{9.0}O_{23}(H_2O)_{9.8}$ as compared to okenite, $Ca_5Si_9O_{23}(H_2O)_9$. The mineral formula of the crystallized gel of Cole and Lancucki, based on 32 anions, was computed to be $(Ca, Na, K)_{5.2}(Si, Al)_{10.4}O_{23}(H_2O)_{7.3}$. The mineral formula of the crystallized gel from the battery, based on 22 anions, was computed to be $(Ca, Na, K)_{3.7}(Si, Al)_{6.2}O_{15}(H_2O)_{6.7}$ as compared to nekoite, $Ca_3Si_6O_{15}(H_2O)_7$, a closely related mineral to okenite. The mineral formula of the crystallized gel of Cole and Lancucki, based on 22 anions, was computed to be $(Ca, Na, K)_{3.5}(Si, Al)_{7.2}O_{15}(H_2O)_{5.0}$.

The XRD pattern collected from the crystallized gel from Battery Farnsworth is very similar to the XRD pattern reported by Cole and Lancucki for crystallized gel heated in an oven for 2 h at 110 °C, and allowed to rest at room conditions for 12 days [13]. Cole and Lancucki refer to the crystallized gel as the 10.6 and 8.85 Å phase. The 10.6 and 8.85 Å phase described by Cole and Lancucki lacks the primary okenite peak at 21 Å. Cole and Lancucki assert that the 21 Å peak of okenite "essentially disappears in a lightly ground sample" and "is not vital to the identification of the 10.6 and 8.85 Å phase as okenite". Due to the size of the aperture, as shown in Fig. 10, *d*-spacings greater than 12.5 Å were not recorded, thus the presence or absence of the 21 Å peak could not be determined from the XRD pattern for the crystallized gel from the battery. The XRD patterns of the crystallized gel from the battery, and the 10.6 and 8.85 Å phase described by Cole and Lancucki, are very similar to each other, and share some of the major peaks of okenite, but do not correspond directly to the *d*-spacings listed for okenite.

EDX measurements of the amorphous gels showed decreased concentrations of K and Na, and increased concentration of Ca as compared to the crystallized gel. Amorphous gel immediately adjacent to the crystallized gel tended to have higher concentrations of K and Na, and a lower concentration of Ca than amorphous gel within the cement paste. The measurements of the amorphous gels were more variable than the measurements from the crystallized gel.

Since no fresh samples of hardened concrete from the battery were examined in this study, it cannot be definitively shown that the crystallized gels observed are not simply the result of crystallization due to the air dried state of the samples.

Table 4a
Comparison between *d*-spacings reported by Cole and Lancucki [13] for crystallized gel, *d*-spacings from crystallized gel collected from Battery Farnsworth, and *d*-spacings for okenite

Okenite ICCD PDF 33–305		Nekoite ICCD PDF 31–303		Battery Farnsworth, crystallized gel		Cole and Lancucki, heated 110 °C for 2 h and stored in air 12 days [13]		Cole and Lancucki, pure sample [13]	
d-spacing (angstroms)	Intensity	*d*-spacing (angstroms)	Intensity	*d*-spacing (angstroms)	Intensity	*d*-spacing (angstroms)	Intensity	*d*-spacing (angstroms)	Intensity
21	100								
10.7	30			10.59	Major	10.59	32	10.05	20
8.84	80	9.1	100	8.35	Maximum	8.85	70	8.54	100
7.65	35	7.37	20					7.08	22
6.73	35	6.64	65	6.44	Major	6.63	27	6.63	22
6.23	16								
5.794	15	5.81	10						
5.589	10	5.64	19						
5.355	12	5.54	25					5.51	8
4.99	4							5	
4.672	8								
4.539	25	4.55	20						
4.422	14	4.46	10						
4.35	18			4.26	Major	4.23	27	4.25	8
4.164	12	4.17	12						
4.113	10								
3.969	10	3.92	10						
3.841	4	3.824	10						
3.691	3	3.686	7						
		3.64	5						
3.594	25	3.58	5	3.57	Major	3.59	68	3.56	60
3.493	10	3.552	5						
3.387	20	3.449	20						
3.343	13	3.381	55	3.34	Maximum	3.35	100	3.35	67
3.298	8	3.319	90						
3.252	6	3.296	55						
3.219	13	3.242	15						
3.167	19								
3.113	55	3.123	12					3.11	12
3.069	30	3.029	20						
3.002	55	2.953	18			3.02	22	2.98	38
2.95	60	2.93	20						
2.923	60	2.9	9	2.92	Major	2.93	59	2.92	56
2.85	25	2.88	10						
		2.829	55						
2.801	45	2.803	55						

However, considering the age of the concrete and the abundance of crystallized gel, it is reasonable to postulate that over an extensive period of time, on the order of decades, alkali silica gel rich in alkalies will crystallize.

The reactivity of the quartz rich metasedimentary coarse aggregate used in the concrete is likely related to the Na and K contents of the cements used. No detailed mix design information is included in Perrault and Ofenstein's report on the construction and history of the battery [3]. However, the report does include a short excerpt of the inspector's notes with a description of a test batch of concrete. According to the notes, a cubic foot of cement powder (loose) weighed 80 lbs (approximately 1.3 g/c^3) and a test batch consisting of 1 ft^3 of cement, 2 ft^3 of sand, and 4 ft^3 of rock, after dry mixing, weighed 605 lbs. (275 kg) [3]. After mixing with water, and ramming into a box, the concrete occupied a volume of 4.2 ft^3, (a cement content of 306 kg/m^3) [3]. Using the cement alkali levels listed in Table 1, this translates into a concrete alkali content of 20.8 kg/m^3 if Hoffman Cement was used, and a concrete alkali content of 5.5 kg/m^3 if Atlas Cement was used. Both values exceed modern recommendations for protection against alkali silica reactivity, so the extent of the alkali silica reaction observed in the battery is not surprising.

Acknowledgements

Thank you to Pete Payette of the American Forts Network, and Bolling Smith of the Coast Defense Study Group, Inc., for permission to use current and historic images of the battery. Thank you to Fred Bailey, who recorded the diffraction pattern used in this paper.

References

[1] P. Payette, P. Payette, History of Fort Constitution, American Forts Network, North American Fortifications,/2004/,[Online] Available at: http://www.geocities.com/Fort_Constitution/history.html.

Table 4b
Comparison between *d*-spacings reported by Cole and Lancucki [13] for crystallized gel, *d*-spacings from crystallized gel collected from Battery Farnsworth, and *d*-spacings for okenite and nekoite

Okenite ICCD PDF 33–305		Nekoite ICCD PDF 31–303		Battery Farnsworth, crystallized gel		Cole and Lancucki, heated 110 °C for 2 h and stored in air 12 days [13]		Cole and Lancucki, pure sample [13]	
d-spacing (angstroms)	Intensity	*d*-spacing (angstroms)	Intensity	*d*-spacing (angstroms)	Intensity	*d*-spacing (angstroms)	Intensity	*d*-spacing (angstroms)	Intensity
2.708	8	2.788	40						
2.622	4	2.769	50			2.65	5		
2.553	12	2.609	3			2.51	5		
2.459	7	2.484	10	2.45	Minor	2.45	5	2.46	8
2.422	13	2.464	30						
2.39	17	2.438	19						
2.345	8	2.355	10						
2.321	12	2.292	5						
2.253	12	2.27	5	2.28	Minor	2.27	5		
2.216	13	2.204	3						
2.161	13	2.189	13						
2.1	2	2.068	3	2.12	Minor			1.98	4
2.034	4								
2.001	7								
1.975	3								
1.94	7	1.936	7						
1.915	7	1.91	7						
1.898	20								
1.85	4	1.83	75						
1.82	70	1.794	15	1.82	Minor	1.78	18	1.82	16
		1.789	15						
1.777	12	1.776	20	1.76	Minor				
1.747	3	1.752	9	1.67	Minor				
1.695	4	1.691	5	1.54	Minor				
		1.661	3	1.38	Minor				
		1.646	4						
		1.62	10						
1.597	8	1.604	12						
1.569	8	1.579	5						
1.55	10	1.563	4						
1.533	12	1.541	17						
1.512	6								
1.455	6	1.46	5						
1.429	3	1.44	8						
		1.389	9						
		1.354	10						

[2] G. Williford, S.K. Ofenstein, C.L. Perrault, Contextual history of the coastal fortifications at Fort Point, in: Walbach Tower, Battery Farnsworth, Associated Structures and Environs, Fort Point, New Castle, New Hampshire Integrated Cultural Landscape Report and Historic Structure Report, Section 1, draft version, 2005, 1–146, [Online] Available at: http://facilities-dc.sr.unh.edu/Project_Files/briefcase/mrf/Fort_Point_HSR/FortPointHSR-Part1-DRAFT1-13-2005.pdf.

[3] C.L. Perrault, S.K. Ofenstein, Construction and developmental history of structures, in: Walbach Tower, Battery Farnsworth, Associated Structures and Environs, Fort Point, New Castle, New Hampshire Integrated Cultural Landscape Report and Historic Structure Report, Section 3, draft version, 2005, 181–492, [Online] Available at: http://facilitiesdc.sr.unh.edu/Project_Files/briefcase/mrf/Fort_Point_HSR/FortPointHSR-Part1-DRAFT1-13-2005.pdf.

[4] U. Cummings, American Cements, Rogers & Manson, Boston, USA, 1898.

[5] C.E. Eckel, Cements, Limes, and Plasters, 1st edition, John Wiley & Sons, New York, USA, 1905.

[6] M.S.J. Gani, Cement and Concrete, 1st edition, Chapman and Hall, London, UK, 1997.

[7] L.C. Sabin, Cement and Concrete, McGraw Publishing Company, New York, USA, 1905.

[8] F.H. Lewis, The plant of the Lawrence Cement Company, Binnewater, N. Y. The Cement Industry— Descriptions of Portland and Natural Cement Plants in the United States and Europe, with Notes on Materials and Processes in Portland Cement Manufacture, The Engineering Record, New York, USA, 1900, pp. 151–160.

[9] F.H. Lewis, The American rotary kiln process for portland cement, The Cement Industry— Descriptions of Portland and Natural Cement Plants in the United States and Europe, with Notes on Materials and Processes in Portland Cement Manufacture, The Engineering Record, New York, USA, 1900, pp. 188–199.

[10] E.J. Hadley, The Magic Powder, G.P. Putnam's Sons, New York, USA, 1945.

[11] E. Foulds, L. Laham, S.K. Ofenstein, C.L. Perrault, Developmental history of the landscape at Fort Point, in: Walbach Tower, Battery Farnsworth, Associated Structures and Environs, Fort Point, New Castle, New Hampshire Integrated Cultural Landscape Report and Historic Structure Report, Section 2, draft version, 2005, 151–176, [Online] Available at: http://facilities-dc.sr.unh.edu/Project_Files/briefcase/mrf/Fort_Point_HSR/-DRAFT1-13-2005.pdf.

[12] M. Regourd, H. Hornain, B. Mortureux, Microstructure of concrete in aggressive environments, in: P.J. Sereda, G.G. Litvan (Eds.), Durability of Building Materials and Components, ASTM STP 691, American Society for Testing and Materials, Philadelphia, USA, 1980, pp. 253–268.
[13] W.F. Cole, C.J. Lancucki, Products formed in an aged concrete: the occurrence of okenite, Cem. Concr. Res. 13 (1983) 611–618.
[14] G. Samuel, A.K. Mullick, S.P. Ghosh, R.C. Wason, Alkali silica reaction in concrete— SEM and EDAX analyses, Proceedings of the Sixth Annual International Conference On Cement Microscopy, Albuquerque, New Mexico, USA, 1984, pp. 276–291.
[15] G. Davies, R.E. Oberholster, The alkali-silica reaction product: a mineralogical and an electron microscopic study, Proceedings of the Eighth Annual International Conference On Cement Microscopy, Orlando, Florida, USA, 1986, pp. 303–326.
[16] G. Davies, R.E. Oberholster, Alkali-silica reaction products and their development, Cem. Concr. Res. 18 (1988) 621–635.
[17] K. Thordal Andersen, N. Thaulow, The study of alkali-silica reactions in concrete by the use of fluorescent thin-sections, in: B. Erlin, D. Stark (Eds.), Petrography Applied to Concrete and Concrete Aggregates, ASTM STP 1061, American Society for Testing and Materials, Philadelphia, USA, 1990, pp. 71–89.
[18] N. Thaulow, U. Hjorth Jakobsen, B. Clark, Composition of alkali silica gel and ettringite in concrete railroad ties: SEM-EDX and X-ray diffraction analyses, Cem. Concr. Res. 26 (2) (1996) 309–318.
[19] K.E. Kurtis, P.J.M. Monteiro, J.T. Brown, W. Meyer-Ilse, In Situ Alkali-Silica Reaction Observed by X-ray Microscopy, The Center for X-ray Optics, Lawrence Berkeley National Laboratory, Advanced Light Source Abstracts, 1997, [Online] Available at: http://www.cxro.lbl.gov/microscopy/ALS_Abstracts_97/ALS_Abstract_SilicaGel97a.html.
[20] K.E. Kurtis, P.J.M. Monteiro, J.T. Brown, W. Meyer-Ilse, Expansive reactions in concrete observed by soft X-ray transmission microscopy, Mater. Res. Soc. Symp. Proc. 524 (1998) 3–9.
[21] A. Fernandez-Jimenez, F. Puertas, The alkali-silica reaction in alkali-activated granulated slag mortars with reactive aggregate, Cem. Concr. Res. 32 (2002) 1019–1024.
[22] I. Fernandes, F. Noronha, T. Madalena, Microscopic analysis of alkali-aggregate reaction products in a 50-year-old concrete, Mater. Charact. 53 (2004) 295–306.
[23] S.L. Sarkar, D.G. Zollinger, K. Mukhopadhyay, L. Seungwook, Appendix 1— Handbook for Identification of Alkali-Silica Reactivity, Airfield Pavement, Advisory Circular No. 150/5380-8, U.S. Department of Transportation Federal Aviation Administration, 2004, [Online] Available at: http://www.faa.gov/arp/publications/acs5380-8.pdf.
[24] J.W. Anthony, B.A. Richard, K.W. Bladh, M.C. Michols, Handbook of Mineralogy, Volume II— Silicates, Mineralogical Society of America, Mineral Data Publishing, version 1.2, 2001, [Online] Available at: http://www.minsocam.org/MSA/Handbook/.
[25] W.A. Deer, R.A. Howie, J. Zussman, An Introduction to the Rock-Forming Minerals, 2nd edition, John Wiley & Sons, New York, USA, 1992.